

Finite Element Analysis on the Mechanical Properties of the Fundamental Elements of a Frame-Truss Composite Wall

Li Xiaolei^a, Lu Junlong^{*a}, Zhang Chao^b

^aSchool of Civil Engineering and Architecture, Xi'an university of Technology, xian 710048, China

^bShaanxi Zhong Lin Group for Engineering Design and Research Co Ltd, xian 710055, China
 lujunlong@sohu.com

To address existing problems of lateral force resisting systems, the paper proposed the concept of a novel frame-truss composite wall. With the intention of testing its seismic performance, the finite element software ABAQUS was used to establish a nonlinear finite element model of the fundamental elements of the wall. By taking material nonlinearity into account, and with a simulative load test, the paper analysed the force performance of the wall elements. Specifically, the finite element analysis was first conducted on the embedded steel-rib short-leg shear wall, whose results agreed well with the test result. Thus the model was reliable. Then, on this basis, the paper analysed the influential factors of the failure mode and bearing capacity. Finally, the paper provided reasonable parameters for the fundamental elements of the novel wall, which lay foundation for further research.

1. Introduction

The improvement of seismic performance of buildings is an effective way to enhance comprehensively earthquake resistance and disaster prevention in earthquake zones on the one hand, and to reduce the number of casualties and material loss as well in earthquake areas on the other hand. The lateral force resisting system that satisfies the anti-seismic requirements of the structure with it is supposed to have suitable stiffness, relatively good damping, and superior ductility. In order to meet these demands at the same time when the building function is achieved, for the reinforced concrete based anti-seismic constructions with columns, walls, or tubes as the main members or systems in terms of lateral force resistance, it is suggested that the construction components' cross section and reinforcing bar should be adjusted properly, and that the suitable structure layout is adopted to the construction. The lateral force resisting system of frame structures has low stiffness and limited bearing capacity; and the lateral force resisting system of shear walls and tubular structures as well has higher stiffness and stronger carrying capacity by comparison. However, for the latter one, in order to match the ductile demand, it is required that the structure should be designed with openings such that coupling beams will form. Not only that stiffness of the structure should be properly adjusted, but shear walls or the walls of tubular structures are difficult to restore once broken in earthquakes.

(Yao et al., 2004) presented the multi-ribbed composite wall along with an all-around analysis of the theory and calculation method of this new type of anti-seismic structural design. (Dong et al., 2013) proposed energy-saving block and invisible multi-ribbed frame wall. As an early-stage common approach to fortifying anti-seismic structures in Japan, to integrate reinforced concrete based shear walls with a structure was characterized by large flexural rigidity and strong lateral force resistance. Shear walls thus became the dominant member of lateral load resistance for frame-shearing wall structures. However, with poor ductility, this structure tended to crack under strong earthquakes, thus the rigidity was lowered down. As a result, it was replaced with grid walls, as is shown in Figure 1(a), with good decorative, lighting, and ventilating effects. Grid walls were then applied to fortify constructions. As the concrete is directly encased by steel skeletons, the adhesive force between the concrete and the steel skeleton is relatively large; the stiffness of gird rod pieces turns out to be overmuch; as a consequence, the gird wall tends to undergo brittle fracture under the action of earthquakes. In addition, as can be seen from Figure 1, each of the grid in the grid wall is rhombic; if a connected node of the rod piece yields, the node will be hingedly jointed rather than rigidly jointed, and the

originally rhombic grid will change into geometrically unstable system. Therefore, on this basis, (Li, 2015) proposed the idea of a novel composite wall that can be assembled, and called it as frame-truss composite wall, as shown in Figure 1(b). When fixed to RC frames, this wall is easy to adjust the stiffness, with low energy consumption and adorable lighting effect. The proposed frame-truss composite wall has a bright prospect due to broad application, covering newly-built constructions, fortification for existing buildings, and buildings of earthquake reconstruction.



Figure 1 (a): grid shear wall

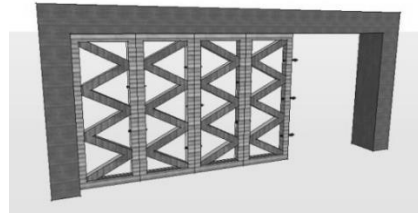


Figure 1 (b): frame-truss composite wall

Grids are the basic load-bearing element of the frame-truss composite wall. The distribution and transmission of grid force is the precondition for determining rational grid failure mode and optimizing grid parameters, and provides the foundation for realizing rational failure mode of the novel wall. The complicated grid structure is greatly different from the construction of either ordinary walls or lateral force resisting elements. Given this, the paper merely undertook ABAQUS on the wall elements under monotonic loading. With varying values of some parameters (such as embedded steel panel thickness, concrete strength grade, and axial compression ratio), by comparing their different impacts on the failure mode, bearing capacity, and ductility of the wall elements, the paper identified the failure characteristics and relative design parameters of the basic elements. The analysis result lays foundation for further research.

2. Model validation

On account of the novelty, there has been no studies on the composite wall yet. Considering wall materials and the features of force on them, based on ABAQUS, the paper quoted the test on the embedded steel-rib short-leg shear wall as a way to verify the rationality and reliability of the finite element model hereby (WANG et al., 2014). The length-thickness ratio of the wall is 6, the shear-span ratio equals 2.2, the axial compression ratio equals 0.3, and the concrete strength grade is C40.

The stress-strain model developed (Attard and Setunge, 1996) was used to obtain the stress-strain curves for concrete under uniaxial stresses. There are three ways to define the softening behavior of concrete under uniaxial tensions in ABAQUS, among which the failure criteria of concrete was used hereby, namely the stress-fracture energy relationship. The value of the fracture energy (represented by G_f) was computed according to the European Standards CEB-FIP MC 90 (1990).

Concrete used 8-node 3D entity elements in the form of reduced integration C3D8R, and steel panels used 4-node shell elements in the form of complete integral S4. To reach certain computation precision, the paper employed 5-node Simpson integral along the thickness of the shell elements. 3D linear Truss T3D2 is used both for longitudinal bars and stirrups. Only the axial action was considered hereby. Shear force and bending power were excluded. Other relative parameters were: angle of dilation, 30° ; eccentricity, 0.1; the ratio of biaxial ultimate compressive strength to uniaxial ultimate compressive strength, 1.16; the second stress invariant of the stress-strain meridian plane, 0.6667; the viscous coefficient, 0.0002; and the recovery coefficient of concrete, 1.0. The viscosity displacement between steel panels and concrete was excluded. The relationships between steel panels and concrete, and between reinforcing bars and concrete were both defined as embedded.

The lower part of the test sample acted as the fixed end, and was coupled with RP-5, the reference point. The degrees of freedom in six directions were confined. The load beam was tied to the upper part of the sample under it. There was a reference point RP-3 on the upper part of the load beam, which was coupled with the sample so as to control the axial compression ratio. 10mm ahead of the load beam was the reference point RP-4, which passed the center of the load beam, and was coupled with the load beam by Rigid body. The displacement loading system was used, where the displacement boundary was set as 45mm.

Figure 2 is the comparison of skeleton curves between the simulative load displacement and the tested one. As can be seen, the elastic stiffness of the ABAQUS curve is higher than that of the tested curve. The reason is that the given concrete by the finite element analysis is ideally homogeneous, while the tested one is nonhomogeneous, let alone certain defects in the sample. The sample for the test is under cyclic loading,

whilst the sample for the finite element analysis is under monotonic loading. Also, the viscosity displacement between the concrete and the reinforcing bar is excluded here. Despite the differences, the simulative result agrees well with the test result, because both of them have similar peak loads and the corresponding displacements, and ultimate loads and the corresponding displacements as well, which can be seen from Table 1 and Figure 2. This demonstrates that the material constitutive relationship and the parameters selected for the finite element analysis can relatively accurately simulate test results. The precision of the finite element result shows that the established model in the paper is effective.

Table 1: comparison between the test and the simulation

Specimen	Yield load	Yield displacement	Peak load	Peak displacement	Ultimate displacement	Ductility coefficient
TEST	345 kN	8.9mm	473 kN	19.82 mm	34.4 mm	3.87
ABAQUS	417 kN	10.86 mm	480 kN	17.86 mm	38.2 mm	3.52

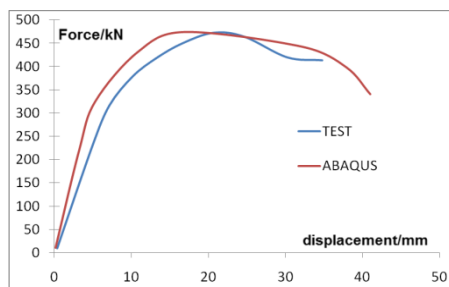


Figure 2: The comparison of skeleton curves between simulative and test

3. Finite element modeling and parameter analysis

Below is the nonlinear analysis on the basic wall elements under monotonic loading by changing values of different parameters. In order to research into the features of force on elements, the paper established the ABAQUS model. Since the failure law of different elements is uniform, the paper took stochastically one element as an example to expound its failure process, and analysed the influential factors of the force on it by changing values of different parameters. Figure 3 is the model structure. A uniformly distributed load was applied vertically to the top of the load beam, and displacement control was exerted horizontally.

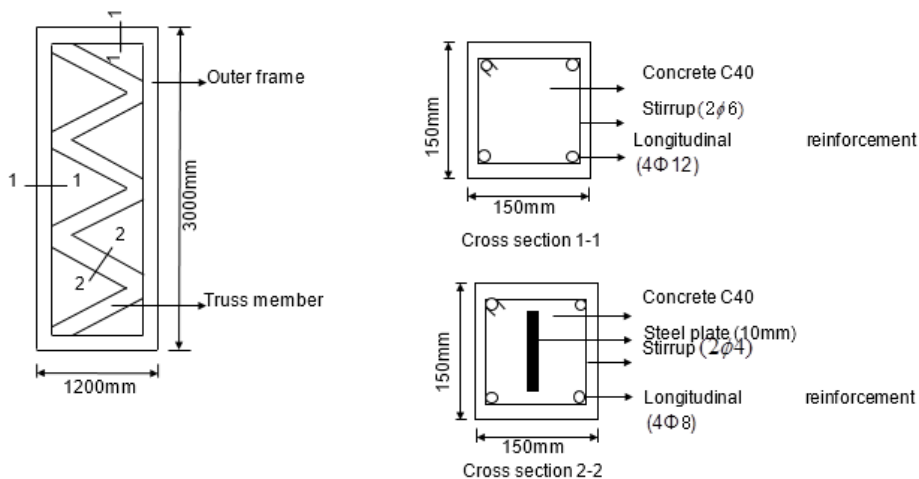


Figure 3: Element size and its cross section

The computation results are shown in Figure 4 (a-e), which are successively compressive damage of concrete (damagc), vertical displacement of concrete (U1), concrete Mises stress, embedded steel panel Mises stress, and the diagram of final damage and deformation. According to the simulative result, based on material yield and damage stress, it can be known that the failure mode of the novel wall is bending failure. The final

damage falls on the concrete on the pressure side of the frame bottom, which is crushed. The truss rod is less stressed, so only the bottom of the truss rod is broken finally.

To further study the force performance of the wall element, considering the influence of some major parameters on the wall element, the paper chose four major parameters (concrete strength grade, steel panel thickness, axial compression ratio, and reinforcement ratio of longitudinal bars) for analysis.

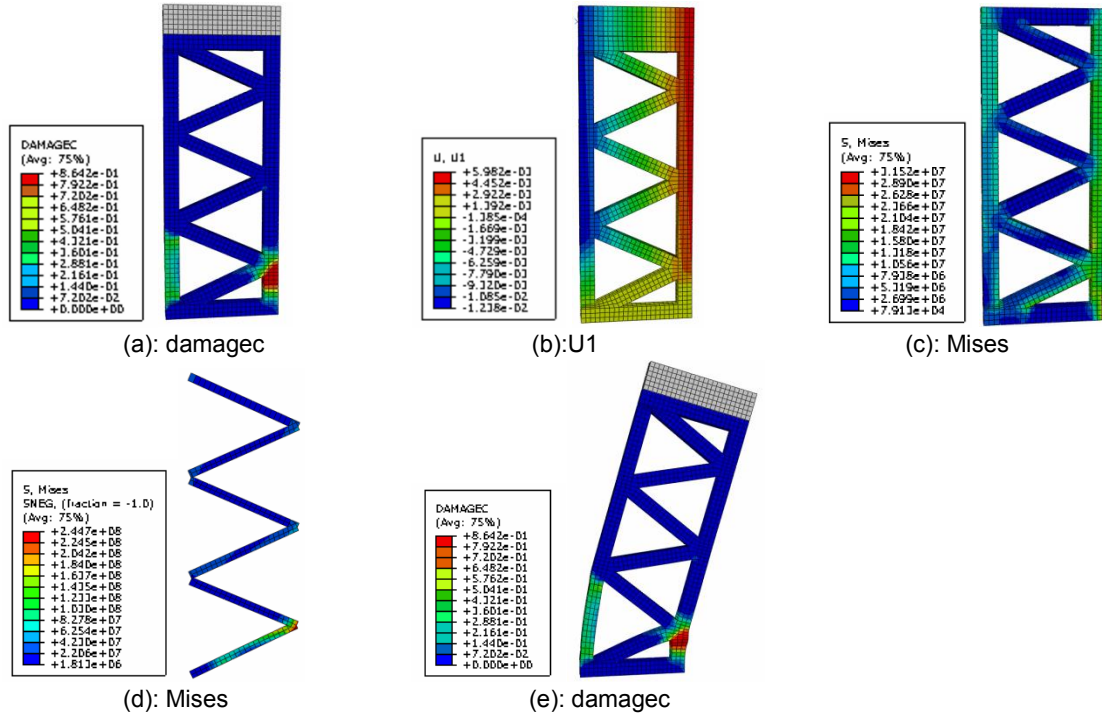


Figure 4: The calculation results of numerical calculation

3.1 The influence of concrete strength grade

Concrete strength grade is the only variable, and the value of the rest parameters remain constant. Figure 5 (a) is the skeleton curve of concrete models with different strength grades. Through calculating, the paper obtained the changing condition of the ultimate bearing capacity of the wall element as shown in Table 2. As can be seen, the ultimate bearing capacity increased substantially with increasing concrete strength grades under lower axial compression force. However, the concrete strength grade exerts little impact on the ultimate bearing capacity under higher axial compression force.

Table 2: The ultimate bearing capacity of the wall element

Concrete strength grades	C30-1	C40-1	C50-1	C30-2	C40-2	C50-2
Axial compression force(N/mm ²)	2.86	2.86	2.86	5.72	5.72	5.72
Peak load(kN)	86.916	94.331	115.57	115.473	108.554	116.462
Relative value	1.0	1.085	1.33	1.0	0.94	1.01

3.2 The influence of steel panel thickness

The paper chose steel panels of five different thickness, namely 4mm, 6mm, 8mm, 10mm, and 16mm. The reinforced rate for each of them is about 1.33%, 2%, 2.67%, 3.33%, and 5.33%, respectively. Figure 5 (b) is the skeleton curve of concrete models with different thickness of the steel plate. According to computation results, when the concrete strength grade remains unchanged, the influence of steel panel thickness on either the ultimate bearing capacity or the ductility is not large. Thus, for wall samples with the same height-width ratio, the diagonal bracing will not be damaged. Thickness of the steel plate merely impacts on the stress, but will not affect the failure mode.

Table 3: The ultimate bearing capacity of the wall element

Concrete strength grades	C30			C40			C50	
The thickness of the steel plate	4mm	6mm	8mm	6mm	10mm	10mm	16mm	
Peak load(kN)	87.11	87.07	86.92	94.33	90.54	115.57	116.46	
Relative value	1.0	1.0	0.998	1.0	0.96	1.0	1.008	

3.3 The influence of axial compression ratio

Three axial compression ratios were considered hereby, and the uniformly distributed axial compression stress was 2.86N/mm^2 , 5.72N/mm^2 and 8.58N/mm^2 , respectively. C30, C40 and C50 as three concrete strength grades were taken into account. Figure 5 (c) is the skeleton curve of concrete models with different axial compression ratios. By calculation, as the concrete strength grade remains fixed, the axial compression stress exerts great impact on the ultimate bearing capacity and the ductility. The ultimate bearing capacity increased slightly with increasing axial compression stress, while the ductility decreased as the axial compression stress increased.

Table 4: The ultimate bearing capacity of the wall element

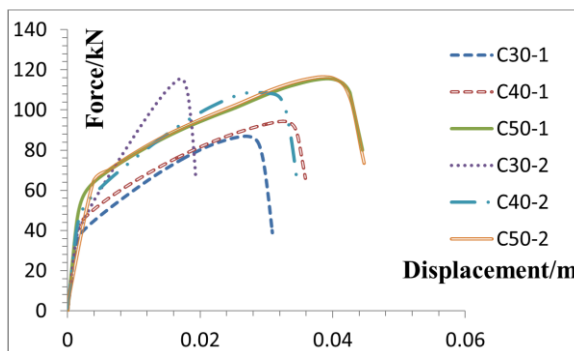
Concrete strength grades	C30			C40			C50	
Axial compression force(N/mm^2)	2.86	5.72	8.58	2.86	5.72	8.58	5.72	8.58
Peak load(kN)	86.665	112.339	122.336	90.54	106.92	133.68	115.57	139.64
Relative value	1.0	1.3	1.41	1.0	1.181	1.476	1.0	1.208

3.4 The influence of reinforcement ratio of longitudinal bars

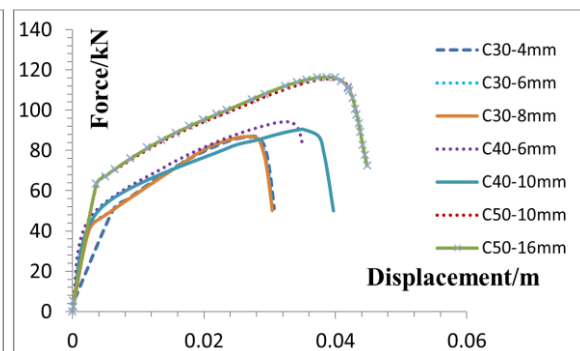
The paper considered two reinforcement ratios of longitudinal bars. The diameters of the longitudinal bar for the external frame are 16mm and 12mm, respectively; and the diameters of the corresponding truss rod are 12mm and 8mm, respectively. For element with concrete strength grades C30 and C40, the uniformly distributed axial compression stresses are 5.72N/mm^2 , and for one with C50, the uniformly distributed axial compression stresses are 5.72N/mm^2 and 8.58N/mm^2 , respectively. Figure 5 (d) shows the skeleton curve of concrete models with different reinforcement ratios of longitudinal bars. According to computation, as the concrete strength grade remains unchanged, when the axial compression stress was large, the ultimate bearing capacity increased and the ductility decreased along with the increasing reinforcement ratio of longitudinal bars; when the axial compression stress was small, the ultimate bearing capacity decreased and the ductility stayed basically the same along with the increasing reinforcement ratio of longitudinal bars. Thus, the influence of the reinforcement ratio of longitudinal bars on either the ultimate bearing capacity or the ductility is small when the concrete strength grade and axial compression ratio are the same.

Table 5: The ultimate bearing capacity of the wall element

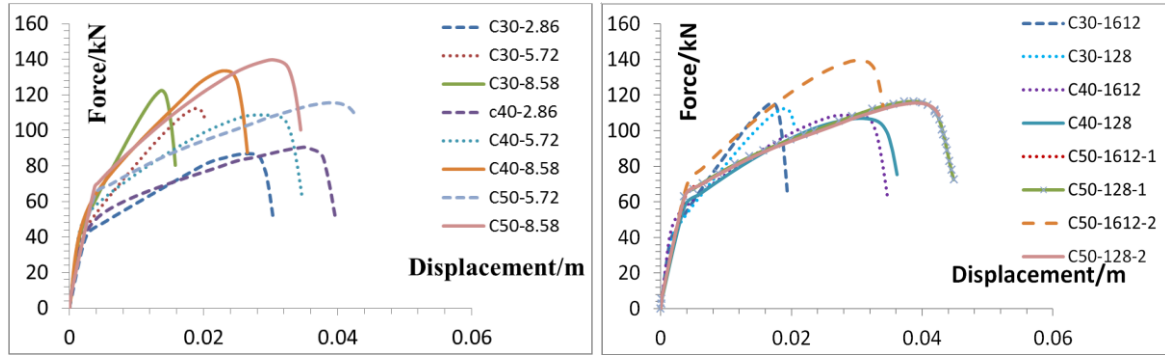
Concrete strength grades	C30		C40		C50-1		C50-2	
Longitudinal reinforcement diameter(mm)	16/12	12/8	16/12	12/8	16/12	12/8	16/12	12/8
Peak load(kN)	115.473	112.339	108.554	106.921	116.462	115.571	139.638	139.639
Relative value	1.03	1.0	1.02	1.0	1.01	1.0	1.0	1.0



(a): with different concrete strength grade



(b): with different thickness of the steel plate



(c): with different axial compression force

(d): with different reinforcement ratio

Figure 5: The skeleton curves of the wall sample with different values of parameters

4. Conclusion

The paper proposes the idea of a novel frame-truss composite wall, and uses ABAQUS to establish a corresponding nonlinear finite element model. By analyzing the failure law, bearing capacity, and ductility of the wall element, this paper shows the conclusions as follow:

The height-span ratio of the composite wall is 2.5. The failure mode is bending failure. The final damage falls on the concrete on the pressure side of the frame bottom, which is crushed. The truss rod is less stressed, so only the bottom of the truss rod is broken finally. Four major parameters (concrete strength grade, steel panel thickness, axial compression ratio, and reinforcement ratio of longitudinal bars) are used to analyze the force performance of the wall element. As can be seen, concrete strength grade, axial compression ratio, and reinforcement ratio of longitudinal bars impact on the ultimate bearing capacity significantly; whilst the impact of steel panel thickness is negligible. The ultimate bearing capacity increased substantially with increasing concrete strength grade. As the concrete strength grade remains the same, the axial compression stress exerts great impact on the ultimate bearing capacity and the ductility. The ultimate bearing capacity increased slightly with increasing axial compression stress, while the ductility decreased as the axial compression stress rose. When the axial compression stress was large, the ultimate bearing capacity increased and the ductility decreased along with the increasing reinforcement ratio of longitudinal bars; when the axial compression stress was small, the ultimate bearing capacity decreased and the ductility stayed basically the same along with the increasing reinforcement ratio of longitudinal bars.

Acknowledgments

The research is supported by the National Natural Science Foundation of China (51508463), China Postdoctoral Science Foundation (2014M562523XB), Scientific Research Plan Project of Shaanxi Education Department (15JK1510).

References

- Attard M.M., Setunge S., 1996, Stress-strain relationship of confined and unconfined concrete [J]. ACI Materials Journal, 93(5): 432-442.
- CEB-FIP Model Code, 1990, [S]. London: Thomas Telford Services Ltd, 1991.
- Dong J.X., Qian j., Li S.C., 2013, Calculating formulas of elastic constants and lateral rigidity of energy-saving block and invisible multi-ribbed frame wall [J]. Journal of Central South University (Science and Technology), 2013, 44(3): 1144-1151.
- Li X.L., Lu J.L., Zhang C., 2015, Reviewed on the research of lateral force-resisting members and frame-truss composite wall[J], International journal of earth sciences and engineering, v8, n5, 2344-2348
- Qu Z., Zhang L.X., 2013, State of the art and development tendency of seismic retrofit for reinforced concrete structures in Japan [J], Journal of earthquake engineering and engineering vibration, 33(4), 61-74.
- Wang X.Y., Su Y.S., Yan L.B., 2014, Experimental study on seismic behavior of steel reinforced high strength concrete short-pier shear walls with rectangular section[J], Journal of Building Structures, 35(2): 46-54
- Yao Q.F., Huang W., Tian J., 2004, Experimental analyses of mechanical characteristics and seismic performance of multi-ribbed panel wall [J]. Journal of Building Structures, 25(6): 67-74.